Frontiers in Bioscience Landmark

Front. Biosci. (Landmark Ed) **2025**; 30(5): 33488
https://doi.org/10.31083/FBL33488

Original Research

The Role of CEBPD in Oxidative Stress and Angiogenesis Regulation in Endometriosis

Jing Su[1,2], Peipei Tang[3], Jixiang Zhong[2], Rongxue Zhang[2], Huiying Xue[2], Hong Zhang[1,*]

[1]Department of Reproductive Medicine, The Second Affiliated Hospital of Soochow University, 215004 Suzhou, Jiangsu, China
[2]Department of Reproductive Medicine, Huai'an Maternity and Child Health Care Hospital Affiliated to Yangzhou University, 223002 Huai'an, Jiangsu, China
[3]The Digestive and Reproductive System Cancers Precise Prevention Engineering Research Center of Jiangsu Province, Jiangsu College of Nursing, 223002 Huai'an, Jiangsu, China
*Correspondence: szzhanghong126@126.com (Hong Zhang)
Academic Editor: Jordi Sastre-Serra
Submitted: 3 December 2024 Revised: 20 March 2025 Accepted: 10 April 2025 Published: 19 May 2025

Abstract

Background: Endometriosis (EM) is a prevalent gynecological disorder in women. Although the underlying mechanisms have yet to be fully elucidated, EM may be related to oxidative stress. The current research aimed to identify possible pathways that control oxidative stress in EM, thereby providing a theoretical foundation for its clinical diagnosis and treatment. **Methods**: High-throughput RNA sequencing (RNA-seq) data were integrated with GeneCards online data to screen for oxidative stress-related genes and potential targets in EM. The reverse transcription-quantitative polymerase chain reaction (RT-qPCR), Western blotting, and immunohistochemistry assays confirmed the expression of candidate genes. The *in vivo* and *in vitro* effects of CCAAT enhancer binding protein delta (CEBPD, C/EBP-delta) and DNA damage-inducible transcript 4 (DDIT4) on oxidative stress, cell proliferation, and angiogenesis in endometriotic cells were validated using loss- or gain-of-function approaches. **Results**: CEBPD was highly expressed in ectopic and eutopic endometrial tissue from patients with endometriosis. Loss- or gain-of-function experiments showed that CEBPD promoted oxidative stress, cell proliferation, and angiogenesis *in vitro* and *in vivo*. Integration of RNA-seq and online data revealed that *CEBPD* regulates *DDIT4* expression, subsequently increasing oxidative stress, cell proliferation, and angiogenesis in endometriotic cells. Finally, CEBPD and DDIT4 were found to regulate the expression of extracellular signal-regulated kinase 1/2 (ERK1/2) proteins associated with the mitogen-activated protein kinase (MAPK) signaling pathway. **Conclusions**: These results suggest that CEBPD may promote oxidative stress, cell proliferation, and angiogenesis in EM by activating MAPK via DDIT4. Hence, CEBPD may be a potential target for diagnosing and treating EM.

Keywords: endometriosis; CCAAT-enhancer-binding protein-delta; oxidative stress; cell proliferation; angiogenesis

1. Introduction

Endometriosis (EM) is characterized primarily by intense pelvic pain and infertility, and is the most prevalent gynecological condition among reproductive-aged women [1]. The pathogenesis of EM is complex and involves increased cell adhesion, degradation of the extracellular matrix, angiogenesis, proliferation, abnormal cell apoptosis, interference with cell communication, disruption of the immune system, loss of differentiation, alongside other pathophysiological processes [2–4]. However, the mechanism underlying EM remains unclear, and only a few drugs can effectively control this disease. Therefore, investigations of the pathogenic mechanism of EM and the development of novel therapeutic approaches are of great clinical significance.

Oxidative stress arises from the dysregulation of redox homeostasis, characterized by an imbalance between the excessive production of reactive oxygen species (ROS) and the compromised function of antioxidant defense mechanisms. Moreover, ROS and free radicals not only have the potential to induce cellular damage but also contribute significantly to disease progression [5]. Meanwhile, oxidative stress may be crucial in the onset and progression of EM, primarily by affecting the proliferation and damage of endometriotic cells [6]. Notably, oxidative stress is intricately linked to angiogenesis, with effective regulation of oxidative stress contributing positively to this process [7]. However, the specific genes and pathways associated with EM remain largely unidentified. Meanwhile, the advent of next-generation sequencing technology offers a powerful approach for investigating the transcriptomic, genomic, and epigenomic alterations involved in the pathogenesis of EM and for identifying novel pathogenic genes [8–10]. RNA sequencing (RNA-seq) analysis in the present study revealed that expression of CCAAT enhancer binding protein delta (CEBPD, C/EBP-delta) was significantly elevated in endometriosis tissues, suggesting a potential role in the pathogenesis of this EM. CEBPD is an intron-free

protein encoded by the basic (region) leucine zipper (bZIP) transcription factors that bind to DNA through leucine zipper domains and regulate gene expression across various cell types [11]. As a transcription factor, CEBPD has been implicated in tumor growth, metastasis, and treatment resistance [12–14]. A recent study on high-grade serous ovarian carcinoma found that CEBPD enhanced tumor growth by facilitating drug resistance and cell invasion [15]. However, to our knowledge, the role and mechanism of CEBPD in EM have yet to be reported.

This study seeks to elucidate the role of CEBPD in oxidative stress, cell proliferation, and angiogenesis in EM. A thorough analysis of the pathogenesis of EM should help to identify potential diagnostic markers for this disease.

2. Materials and Methods

2.1 Clinical Samples

Eutopic endometrium (EU) and ectopic endometrium (EC) samples were obtained via hysterolaparoscopy from 30 patients diagnosed with EM ovarian cysts combined with infertility. Inclusion criteria for the EM group: (1) aged between 20 and 49 years; (2) regular menstrual cycles with sex hormone tests indicating the follicular phase; (3) confirmed EM diagnosis by laparoscopy and histopathology; (4) application of the revised American Fertility Society (r-AFS) scoring system for laparoscopic diagnosis of EM, with the intraoperative score classified as stage III or IV. During surgery, specimens from endometriotic cyst walls were collected and categorized into the EC group; *in situ* endometrial tissues were collected and categorized into the EU group (n = 30). Normal endometrial (NE) samples were obtained from 30 patients who underwent hysterolaparoscopic surgery for tubal obstruction combined with infertility. Inclusion criteria for the NE group: (1) aged between 15 and 49 years; (2) regular menstrual cycles with sex hormone tests indicating the follicular phase. Exclusion criteria: (1) patients who received hormone therapy within 6 months before surgery; (2) history of thyroid disorders or other metabolic diseases; (3) history of pregnancy or lactation within 6 months before surgery; (4) presence of acute or chronic pelvic inflammatory disease; (5) concurrent gynecological conditions such as uterine fibroids, endometrial polyps, intrauterine adhesions, submucosal fibroids, or gynecological malignancies; (6) history of chronic diseases including cardiovascular disease, hypertension, diabetes mellitus, or other systemic conditions.

After collection, tissue samples were immediately frozen in liquid nitrogen and stored at –80 °C for subsequent analyses using high-throughput RNA-seq, reverse transcription-quantitative polymerase chain reaction (RT-qPCR), Western blotting, and immunohistochemistry.

2.2 RNA Sequencing and Data Analysis

All tissue samples were stored at –80 °C before RNA extraction. Three samples from each group (EU, EC, NE; 9 in total) were chosen for RNA-seq analysis (Majorbio Bio-Pharm Technology Co., Ltd., Shanghai, China). After extracting total RNA, DNase I (2270A, Takara, Shiga, Japan) was used to remove genomic DNA. Subsequently, 1 µg of RNA was used to prepare a transcriptome library for RNA-seq using the TruSeqTM RNA sample preparation kit (Illumina, San Diego, CA, USA). Following mRNA isolation and fragmentation, double-stranded cDNA was synthesized using the SuperScript kit (Invitrogen, Carlsbad, CA, USA) and random hexamer primers (Illumina, San Diego, CA, USA). The cDNA subsequently underwent end-repair, phosphorylation, and the addition of an 'A' base, as per the Illumina library construction protocol. Libraries were sizes elected for cDNA target fragments of 300 bp on 2% Low Range Ultra Agarose followed by PCR amplified using Phusion DNA poly merase (NEB, Ipswich, MA, USA) for 15 PCR cycles. After Quantified by Qubit 4.0 (Q32854, Thermo Fisher Scientific, Waltham, MA, USA), these quencing library was performed on NovaSeq X Plus platform (PE150, Illumina, San Diego, CA, USA) using NovaSeq X Plus Reagent Kit (Illumina, San Diego, CA, USA).

2.3 Cell Culture

The human endometriotic cell line 12Z was acquired from the Institute of Biochemistry and Cell Biology (Jennio-Bio, Guangzhou, China). All cell lines were validated by short tandem repeat (STR) profiling and tested negative for mycoplasma. Cells were grown in Dulbecco's Modified Eagle medium (DMEM)/F12 medium (Gibco, Grand Island, NY, USA) containing 15% fetal bovine serum (CLARK Bioscience, Virginia, Australia) and 1% penicillin–streptomycin (Minibio, Shanghai, China) at 37 °C in a 5% CO_2 incubator.

2.4 CEBPD Overexpression and shRNA Expression

Plasmids were constructed using ProteinBio (ProteinBio Biotechnology, Nanjing, Jiangsu, China). The full-length CEBPD cDNA was cloned into the pCDH-CMV-MCS-EF-copGFP-T2A-Puro vector using EcoRI and BamHI tags. Positive clones were obtained through overlap PCR. Briefly, the *sh-CEBPD-1*, *sh-CEBPD-2*, and scrambled non-targeting shRNA (sh-control) vectors were produced by incorporating *sh-CEBPD-1*, *sh-CEBPD-2*, and scrambled DNAs into the AgeI and EcoRI sites of the pLKO.1-puro vector. To produce lentivirus particles, HEK293T cells were co-transfected with 10 µg of *sh-CEBPD-1* and *sh-CEBPD-2* DNAs, 5 µg of psPAX2, and 10 µg of pMD2.G packaging plasmids using Lipofectamine 2000. Two days after transfection, the supernatants were collected and used to transduce 12Z cells, followed by selection of positive cells. The *sh-CEBPD-1* sequence was CCGACCUCCUCAACAGCAAUCACAA, while the *sh-CEBPD-2* sequence was GCTGTCGGCTGAGAACGAGAA.

2.5 Reverse Transcription-Quantitative Polymerase Chain Reaction

RNA was isolated from tissue samples using an RNA Simple Total RNA kit (DP419, TIANGEN, Beijing, China), per the manufacturer's instructions. Subsequently, RNA was reverse-transcribed into cDNA using a FastKing RT kit with gDNase (KR116, TIANGEN, Beijing, China). Then, the cDNA was subjected to a quantitative polymerase chain reaction (qPCR) using Talent qPCR PreMix (FP209, TIANGEN, Beijing, China) on a CFX96 Touch Real-Time PCR Detection System (BioRad, Herculaneum, CA, USA). The obtained Ct values were normalized to the *GAPDH* housekeeping gene. The forward and reverse primer sequences are listed in **Supplementary Table 1**.

2.6 ChIP-qPCR

Briefly, 1×10^6 cells were washed twice with cold PBS, cross-linked using 1% formaldehyde at room temperature for 10 minutes, and subsequently quenched with glycine (G7126, Sigma-Aldrich, St. Louis, MO, USA) at a final concentration of 125 mmol/L. Chromatin was released following lysis of the cells on ice. The samples were then sonicated, and soluble sheared chromatin was collected. The average DNA length was between 200 and 500 bp. Chromatin samples (20 µL) were stored at –20 °C for input DNA, while 100 µL was used for immunoprecipitation with 10 µg of anti-CEBPD antibody (1:30, #ab245214, Abcam, Cambridge, MA, USA) or IgG antibody (1:50, #2729S, CST, Boston, MA, USA) at 4 °C overnight. The following day, 30 µL of protein beads was added, and the samples were incubated for an additional 3 h. Afterward, the DNA obtained from immunoprecipitation was amplified by PCR using the specific primers shown in **Supplementary Table 1**. The ChamQ SYBR Color qPCR Master Mix (Q411-02, Vazyme Biotech, Nanjing, Jiangsu, China) was used for PCR. Enrichment values were normalized to the input sample and calculated using the $2^{-\Delta\Delta Ct}$ method [16].

2.7 Western Blot Analysis

Western blot analysis was performed according to standard procedures to evaluate the expression of CEBPD, DNA damage-inducible transcript 4 (DDIT4), extracellular signal-regulated kinase (ERK), phospho-ERK (p-ERK), β-actin and HSP90. After blocking with a buffer, the membranes were incubated with the following primary antibodies overnight at 4 °C: CEBPD (1:1000, #ab245214, Abcam, Cambridge, MA, USA), DDIT4 (1:600, 10638-1-AP, Proteintech, Chicago, IL, USA), ERK (1:1000, #ab184699, Abcam, Cambridge, MA, USA), p-ERK (1:1000, #ab229912, Abcam, Cambridge, MA, USA), β-actin (1:1000, #ab8226, Abcam, Cambridge, MA, USA), and HSP90 (1:1000, #ab203085, Abcam, Cambridge, MA, USA). Upon completion of the primary antibody incubation, the membrane was washed three times with an adequate volume of 1× TBST on a shaker. Subsequently, the membrane was incubated with horseradish peroxidase-conjugated secondary antibody (1:4000, #32460, Thermo Fisher Scientific, Waltham, MA, USA) at 37 °C for 1 hour. Finally, the membrane was placed flat in the imaging system, and images were captured using the C400 visible chemiluminescence imaging system (Azure Biosystems, Dublin, OH, USA). The grayscale ratio of the target band to the internal reference was analyzed using ImageJ software (version 1.53t, National Institutes of Health, Bethesda, MD, USA).

2.8 Immunohistochemistry

Tissues were fixed using 4% paraformaldehyde (P0099-3L, Beyotime Biotechnology, Nantong, Jiangsu, China), embedded in paraffin, sectioned into 5 µm slices, and stained with hematoxylin and eosin (H&E) according to standard protocols. Immunohistochemical staining was performed on the tissue sections using anti-human CEBPD (1:200, #ab245214, Abcam, Cambridge, MA, USA) and anti-human DDIT4 (1:100, #10638-1-AP, Proteintech, Chicago, IL, USA). Stained slides were observed by light microscopy, and the images were recorded. The immunoreactivity scores for CEBPD and DDIT4 were determined by multiplying the score for the percentage of positive cells (0: $<$1%, 1: 1–25%, 2: 26–50%, 3: 51–75%, 4: $>$75%) by the score for staining intensity (0: negative, 1: weak, 2: moderate, 3: strong), thus providing a range from 0 to 12.

2.9 Assays for Oxidation Products

Total protein was extracted from 12Z cells after harvesting. The levels of lipid peroxidation, malondialdehyde (MDA), and superoxide dismutase (SOD) activity were assessed using Mn-SOD assay kits (S0103, Beyotime Biotechnology, Nantong, Jiangsu, China) and lipid peroxidation MDA assay kits (S0131, Beyotime Biotechnology, Nantong, Jiangsu, China) according to the manufacturer's instructions. An oxidative stress model was generated by treating 12Z cells with hydrogen peroxide (H_2O_2), and ROS levels were analyzed using flow cytometry.

2.10 Cell Proliferation Assays

A total of 5000 12Z cells were placed into 96-well plates and incubated for 24 h. Thereafter, 10 µL of Cell Counting kit-8 (CCK-8) solution (C0038, Beyotime Biotechnology, Nantong, Jiangsu, China) was added to each well and the plates incubated for the specified period. Cell viability was evaluated at specific time points, and the absorbance was measured at 450 nm using an enzyme immunoassay device.

2.11 Chick Embryo Chorioallantoic Membrane Test

Fresh fertilized eggs weighing approximately 50 to 60 grams were obtained for this study (n = 24). Chick embryos were randomly allocated into four groups: sh-control,

sh-CEBPD, vector control, and OE-CEBPD (n = 6 in each group). Following disinfection and fenestration, the shell membrane was removed, and the eggs were positioned upright in an incubator. Subsequently, 2 million 12Z cells were suspended in 500 µL of serum-free medium and applied onto gelatin sponges, which were then transplanted into the avascular region of the chorioallantoic membrane of 7-day-old chick embryos. A control group was concurrently established to assess the effects of sh-CEBPD-12Z cells and OE-CEBPD-12Z cells on angiogenesis. After 72 h, the sealing tape was carefully removed, and the chick embryo was gently excised circularly to expose the chorioallantoic membrane fully. High-resolution images were subsequently captured using a Canon camera (EOS 5D Mark IV, Canon EF 100 mm f/2.8L Macro IS USM, Ohta-ku, Tokyo, Japan), and the area of angiogenesis in the chick embryo allantoic membrane was quantified using Image-Pro Plus Image analysis software (version 7.0, Media Cybernetics, Rockville, MD, USA).

2.12 5-Ethynyl-2′-deoxyuridine (EdU) Assay

An EdU kit (C0075S, Beyotime Biotechnology, Nantong, Jiangsu, China) was employed for EdU cell proliferation staining. Different groups of cells were collected and suspended, and the density was adjusted after counting. A total of 5×10^4 cells/well were then inoculated into 24-well plates and grown for 48 h. This was followed by incubation with EdU for 2 h, fixation with 4% paraformaldehyde for 15 minutes, and permeabilization using 0.3% Triton X-100 (A600198, Sangon Biotech, Shanghai, China) for 15 minutes. The cells were then incubated with Click Additive Solution for 30 min and finally incubated with Hoechst 33342 for 10 min before image capturing.

2.13 Colony Formation Assay

The colony formation assay involved inoculating 1000 cells into 6-well plates and incubating at 37 °C in a 5% CO_2 environment for two weeks. After fixing using methanol for 30 minutes, the cells were stained with a 0.2% crystal violet solution (C0121, Beyotime Biotechnology, Nantong, Jiangsu, China). A Bio-Rad chemiluminescence imager (Bio-Rad ChemiDoc MP Imaging System, version 6.1, Hercules, CA, USA) was used to capture images, and colonies with >50 cells were counted. Each assay was performed in triplicate.

2.14 Statistical Analysis

SPSS 22.0 (IBM, Armonk, NY, USA) and GraphPad Prism8 (GraphPad Software, San Diego, CA, USA) software were employed for all statistical analyses and graphical images, respectively. Data are presented as the mean ± standard deviation (SD) or mean ± standard error of the mean (SEM). For data conforming to a normal distribution, the expression levels between two groups were compared using Student's *t*-test (two-tailed). In contrast, one-way analysis of variance (ANOVA) was employed to assess the null hypothesis concerning differences between groups, with Tukey's test used for multiple comparisons. Data that were not normally distributed are presented as the median (interquartile range) [M (P25, P75)], with the groups compared using non-parametric tests. Results were considered statistically significant at a value of $p < 0.05$.

Table 1. Comparison of baseline characteristics between NE and EM groups.

Characteristic	NE group (n = 30)	EM group (n = 30)	*p*-value
Age (years)	31.87 ± 2.70	33.57 ± 5.30	0.125
BMI (kg/m^2)	20.52 ± 10.58	22.97 ± 3.23	0.233
FSH (mIU/mL)	7.17 ± 1.88	6.77 ± 1.77	0.408
LH (mIU/mL)	5.37 ± 2.07	4.81 ± 2.67	0.321
E_2 (pmol/mL)	165.99 ± 72.89	131.98 ± 71.66	0.740
CA125 (IU/L)	16.84 ± 9.95	40.41 ± 29.90	<0.001

NE, normal endometrial; EM, endometriosis; BMI, body mass index; FSH, follicle-stimulating hormone; LH, luteinizing hormone; E_2, serum estradiol; CA125, cancer antigen 125.

3. Results

3.1 Patient Baseline Characteristics

A total of 60 patients were enrolled in this study, comprising 30 in the NE and 30 in the EM groups. Table 1 presents a comparison of the baseline characteristics between the two groups. No statistically significant differences in age, body mass index (BMI), or sex hormone levels were noted between the two groups. However, cancer antigen 125 (CA125) levels were significantly higher in the EM group than in the NE group ($p < 0.001$).

3.2 Upregulation of CEBPD in Human EM Tissues

RNA-seq data were obtained from the NE, EU, and EC samples. Genes exhibiting significantly different mRNA expression levels between these tissues were identified by DESeq2 analysis and are represented by volcano plots in Fig. 1. Among the 3756 differentially expressed mRNA transcripts between NE and EC, 2111 were upregulated and 1645 were downregulated (Fig. 1A). In addition, 3334 mRNA transcripts were differentially expressed (1848 upregulated and 1486 downregulated) between EU and EC (Fig. 1B). However, only eight differentially expressed mRNA transcripts were found between NE and EU, of which six were upregulated, meaning two were downregulated (Fig. 1C).

Five genes were differentially expressed in all three group comparisons (NE vs. EC; EU vs. EC; NE vs. EU): *CEBPD*, solute carrier family 5 member 1 (*SLC5A1*), relaxin family peptide receptor 1 (*RXFP1*), LINC03026, and C2 calcium-dependent domain-containing 4B (*C2CD4B*) (Fig. 1D). An intersection analysis of the above genes with the oxidative stress-related gene sets (https://www.genecards.org) revealed that *CEBPD*, *SLC5A1*, and *RXFP1* were

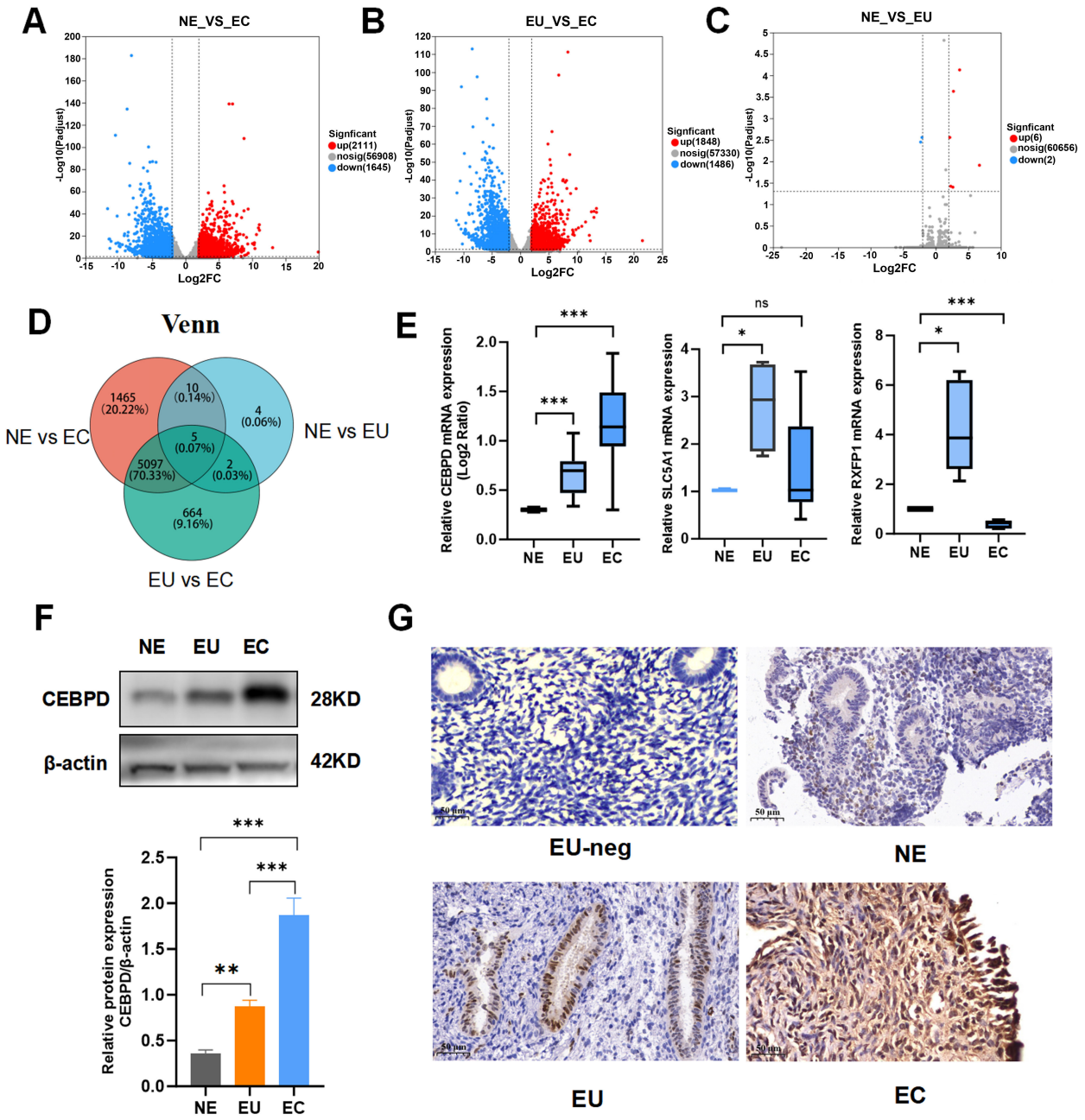

Fig. 1. CEBPD upregulation in human EM tissues. (A) Volcano plot of RNA expression in NE vs. EC dataset (n = 6). (B) Volcano plot of RNA expression in EU vs. EC dataset (n = 6). (C) Volcano plot of RNA expression in NE vs. EU dataset (n = 6). (D) Venn diagram of the commonly expressed RNAs in NE vs. EC, EU vs. EC, and NE vs. EU datasets. (E) Relative *CEBPD*, *SLC5A1*, and *RXFP1* expression levels in NE, EU, and EC tissues as detected by RT-qPCR and normalized to *GAPDH* levels (Log_2-transformed value = $\log_2$ (original value + 1); values shown for *CEBPD* are (M (P25, P75)) from the Kruskal-Wallis test. For *SLC5A1*: NE vs. EU, p = 0.017; NE vs. EC, p = 0.745. For *RXFP1*: NE vs. EU, p = 0.026; NE vs. EC, p = 0.001. Values shown for *RXFP1* and *SLC5A1* are (M (P25, P75)) from the Kruskal-Wallis test; n = 30). (F) CEBPD expression in NE, EU, and EC tissues following Western blotting (NE vs. EU, p = 0.02; NE vs. EC, $p < 0.001$; EU vs. EC, $p < 0.001$; values are the mean ± SD from one-way ANOVA; n = 3). (G) Immunohistochemistry revealed CEBPD upregulation in EC tissues compared with EU and NE tissues. CEBPD is detected in both epithelial and stromal cells. Scale bar = 50 µm. NE, normal endometrium; EU, eutopic endometrium; EC, ectopic endometrium; EU-neg, EU stained without antibody; *CEBPD*, CCAAT enhancer binding protein delta; *SLC5A1*, solute carrier family 5 member 1; *RXFP1*, relaxin family peptide receptor 1; RT-qPCR, reverse transcription-quantitative polymerase chain reaction; ANOVA, one-way analysis of variance. ***$p < 0.001$; **$p < 0.01$; *$p < 0.05$; ns, not significant.

the only common genes. RT-qPCR results confirmed the reliability of high-throughput RNA-seq findings by showing that CEBPD expression was significantly elevated in EC tissue compared to NE (NE vs. EC, $p < 0.001$) and EU (EU vs. EC, $p < 0.001$) tissues (Fig. 1E). Furthermore, Western blotting analysis showed that CEBPD was highly expressed in endometriotic tissues (Fig. 1F). Immunohistochemical analysis demonstrated that CEBPD expression was minimal in normal endometrium. In contrast, immunohistochemical analysis exhibited positive immunoreactivity in both eutopic and ectopic endometria, with significantly enhanced signal intensity observed in the ectopic endometria. Furthermore, immunohistochemical analysis revealed that CEBPD exhibited positive expression in both the nuclei of epithelial and stromal cells (Fig. 1G).

3.3 CEBPD Knockdown Inhibits Oxidative Stress, Proliferation, and Angiogenesis in Endometriotic Cells

To gain more insight into the involvement of CEBPD in the onset and progression of endometriotic lesions, we next evaluated the effects of CEBPD expression on oxidative stress, proliferation and angiogenesis in the 12Z endometriosis cell line (Fig. 2A). Compared with the sh-control group, the MDA levels were significantly reduced in both the sh-CEBPD-1 group (2.43 ± 0.37 vs. 1.28 ± 0.48, $p < 0.001$) and the sh-CEBPD-2 group (2.43 ± 0.37 vs. 1.22 ± 0.51, $p < 0.001$). In contrast, compared with the sh-control group, SOD levels were significantly increased in both the sh-CEBPD-1 group (2.45 ± 0.24 vs. 5.32 ± 0.30, $p = 0.005$) and the sh-CEBPD-2 group (2.45 ± 0.24 vs. 6.50 ± 1.37, $p = 0.001$). Compared with the sh-control group, ROS levels in the oxidative stress cell model were significantly reduced in both the sh-CEBPD-1 group (44.65 ± 3.68 vs. 24.26 ± 1.30, $p < 0.001$) and the sh-CEBPD-2 group (44.65 ± 3.68 vs. 27.67 ± 1.34, $p < 0.001$). These results indicate that CEBPD expression suppression significantly decreased the levels of MDA and ROS in 12Z cells, while concurrently increasing SOD levels (Fig. 2B–D). EdU incorporation, the CCK-8 viability assay, and the colony formation assay all showed that inhibiting CEBPD expression markedly reduced the proliferative capacity of 12Z cells (Fig. 2E,F; **Supplementary Fig. 1A**). In the chick chorioallantoic membrane (CAM) assay, implantation of sh-CEBPD-12Z cells into the avascular region significantly reduced neovascularization due to suppressed CEBPD expression ($p = 0.024$; Fig. 2G).

3.4 CEBPD Overexpression Promotes Oxidative Stress, Proliferation, and Angiogenesis in Endometriotic Cells

We successfully constructed a CEBPD overexpression vector and transfected 12Z cells (Fig. 3A). Compared with the vector group, MDA levels were significantly increased in the OE-CEBPD group (2.70 ± 0.61 vs. 3.80 ± 0.74, $p = 0.013$). In contrast, SOD levels were significantly reduced (2.74 ± 0.67 vs. 1.35 ± 0.20, $p = 0.026$). Additionally, ROS levels in the oxidative stress cell model were significantly increased in the OE-CEBPD group compared with the vector group (36.50 ± 2.54 vs. 64.82 ± 3.30, $p < 0.001$). CEBPD overexpression resulted in significantly increased MDA and ROS levels (Fig. 3B,C), and reduced SOD (Fig. 3D). CEBPD overexpression also promoted cell proliferation (Fig. 3E,F; **Supplementary Fig. 1B**) and angiogenesis ($p = 0.034$; Fig. 3G).

3.5 CEBPD Promotes DDIT4 Expression in Endometriotic Cells

To further investigate the regulatory mechanism of CEBPD in oxidative stress, proliferation, and angiogenesis related to EM, we employed shRNA technology to knock down CEBPD expression in 12Z cells and subsequently conducted RNA-seq analysis. Differentially expressed genes (DEGs) were analyzed to compare the sh-control and sh-CEBPD-1 groups. This analysis revealed 78 DEGs ($|\log_2 FC| \geq 4$), of which 39 were upregulated and 39 were downregulated (Fig. 4A). Furthermore, intersection of the above genes with oxidative stress-related genes with relevance scores ≥ 6 (https://www.genecards.org, **Supplementary Table 2**) identified 10 genes: brain-derived neurotrophic factor (*BDNF*), c-c motif chemokine ligand 5 (*CCL5*), collagen type IV alpha 1 chain (*COL4A1*), DNA damage inducible transcript 4 (*DDIT4*), gamma-glutamyltransferase 1 (*GGT1*), n-myc downstream regulated 1 (*NDRG1*), neurotrophin 3 (*NTF3*), nuclear protein 1, transcriptional regulator (*NUPR1*), S100 calcium binding protein A9 (*S100A9*), and serpin family E member 1 (*SERPINE1*). *DDIT4* gene was selected for further study. RT-qPCR, Western blot, and immunohistochemistry results confirmed that DDIT4 expression was upregulated in the EU and EC tissues. Furthermore, immunohistochemical analysis revealed that DDIT4 exhibited positive expression in both the nucleus and cytoplasm of epithelial and stromal cells (Fig. 4B–D). Primer 5.0 (version 5.0, Premier Biosoft International, Palo Alto, CA, USA) was used to predict the binding site and to design primers to determine whether CEBPD can bind to the *DDIT4* promoter sequence, and three binding sites (D1, D2, D3) were predicted. ChIP-qPCR analysis of the 12Z cell line showed that significantly more DDIT4 was precipitated when using CEBPD antibodies than with IgG antibodies. Moreover, the ChIP assay in 12Z cells confirmed that CEBPD was directly correlated with DDIT4 promoters within D1 and D2, with the most significant binding observed in D2 (Fig. 4E). These data for the D3 region did not meet our stringent quality control criteria and were, therefore, excluded from further analysis. Inhibition of CEBPD expression significantly reduced the DDIT4 mRNA and protein levels in 12Z cells, whereas CEBPD overexpression promoted DDIT4 expression (Fig. 4F–H).

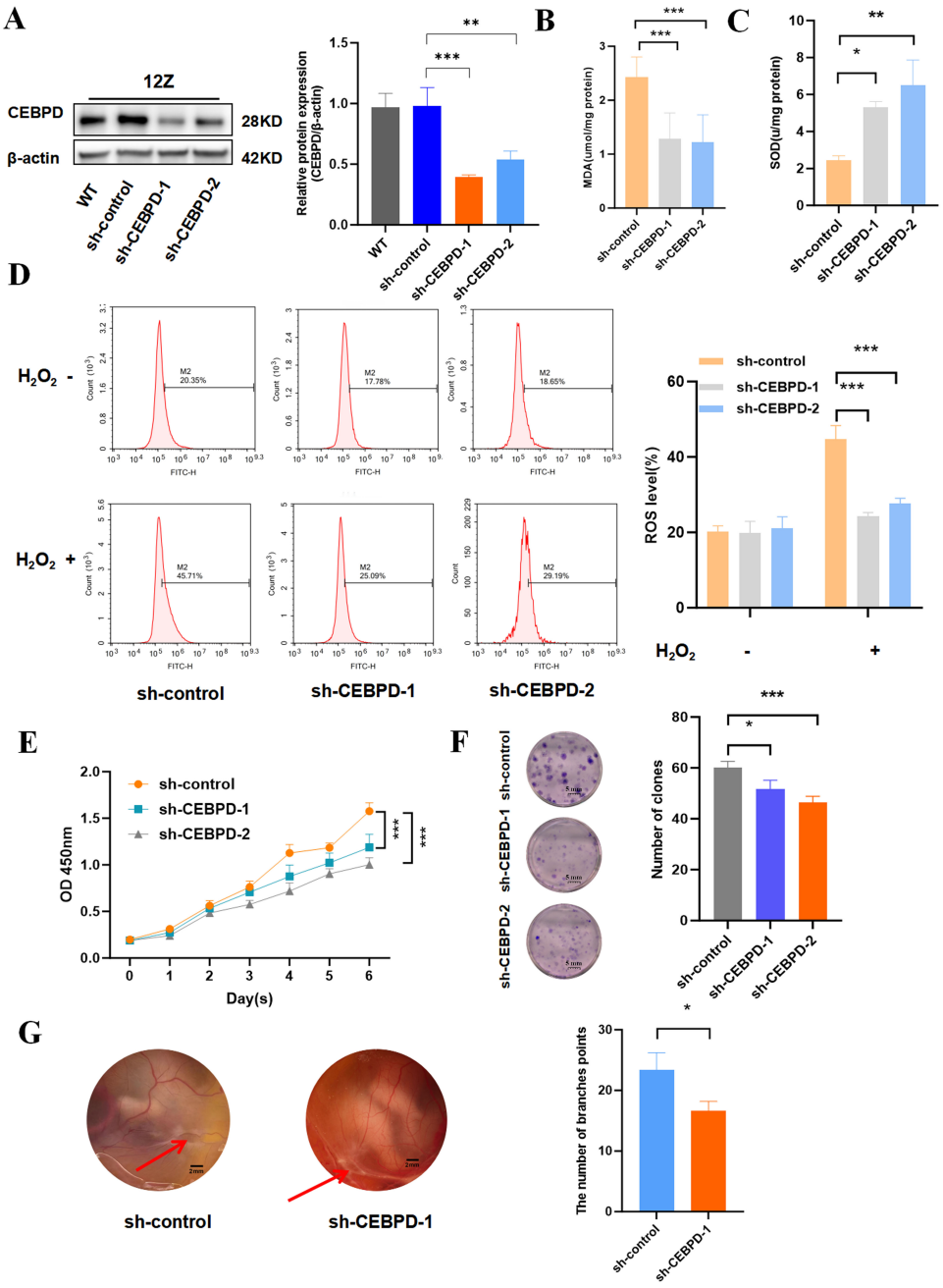

Fig. 2. CEBPD knockdown inhibits oxidative stress, proliferation, and angiogenesis in 12Z cells. (A) Negative control or shRNA (sh-CEBPD #1, #2) was transfected into 12Z cells (sh-control group vs. sh-CEBPD-1 group, $p < 0.001$; sh-control group vs. sh-CEBPD-2 group, $p = 0.01$; values are presented as the mean ± SD from a one-way ANOVA test; n = 3). (B,C) CEBPD expression in 12Z cells was inhibited to evaluate changes in MDA and SOD levels (values are presented as the mean ± SD from one-way ANOVA test; n = 3). (D) The oxidative stress model was constructed using hydrogen peroxide (H_2O_2), and the effect of CEPBD inhibition on ROS levels in 12Z cells was detected by flow cytometry (values are presented as the mean ± SD from a one-way ANOVA test; n = 3). (E) The proliferative capacity of 12Z cells was assessed using the CCK-8 assay, and the results are presented as a line chart (sh-control group vs. sh-CEBPD-1 group, $p < 0.001$; sh-control group vs. sh-CEBPD-2 group, $p < 0.001$; values are shown as the mean ± SD following a one-way ANOVA test; n = 3). (F) The proliferative capacity of 12Z cells was assessed using the clone formation assay, with the bar graphs showing the number of colonies (sh-control group vs. sh-CEBPD-1 group, $p = 0.013$; sh-control group vs. sh-CEBPD-2 group, $p = 0.001$; values are presented as the mean ± SD after a one-way ANOVA test; n = 3). Scale bar = 5 mm. (G) The effects of CEBPD inhibition on angiogenesis were analyzed using the chick embryo chorioallantoic membrane test. Red arrows indicate new blood vessels (values are the mean ± SD following the Student's *t*-test; n = 3). Scale bar = 2 mm. MDA, malondialdehyde; SOD, superoxide dismutase; CCK-8, Cell Counting kit-8. ***$p < 0.001$; **$p < 0.01$; *$p < 0.05$.

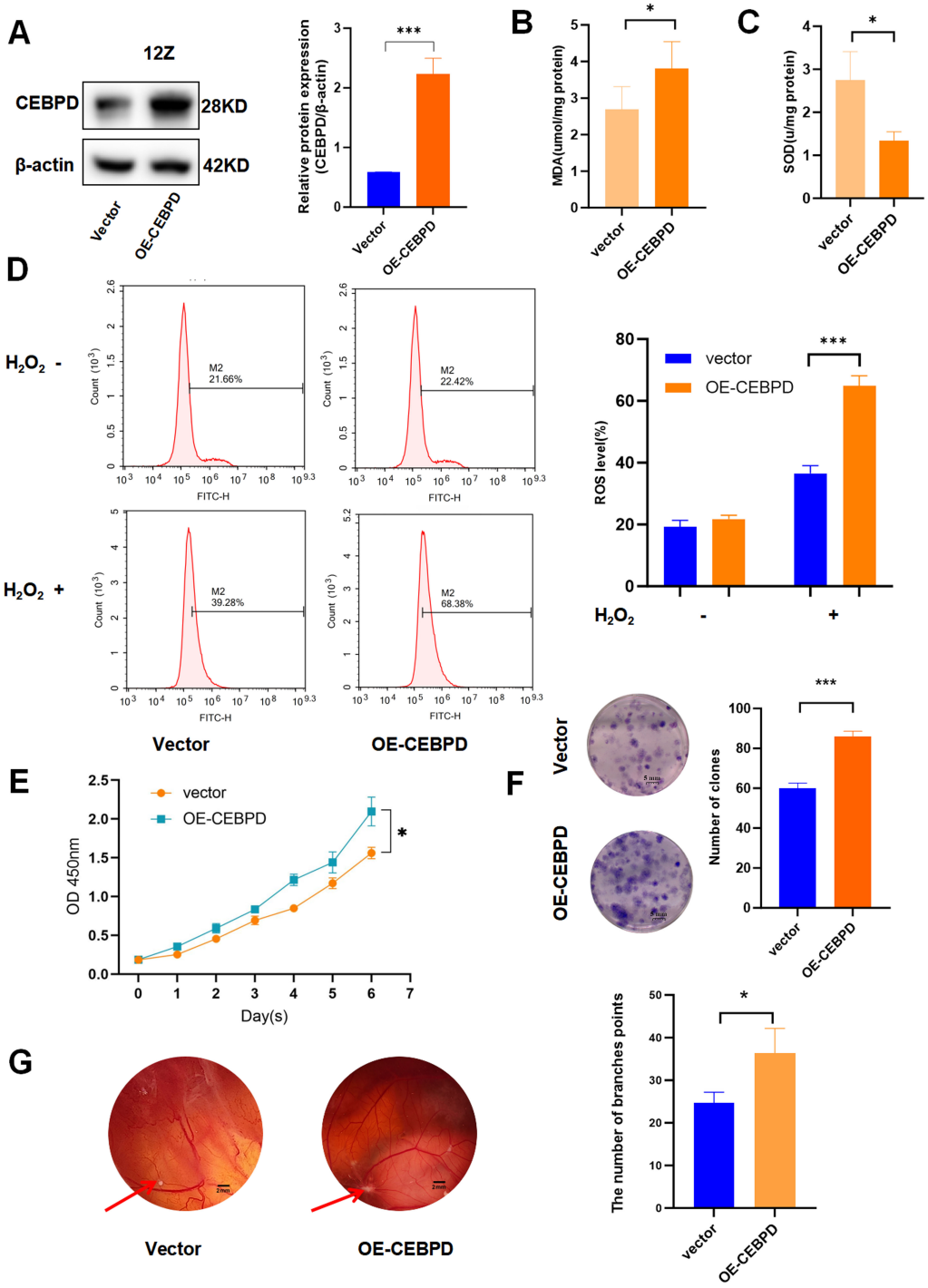

Fig. 3. CEBPD overexpression promotes oxidative stress, proliferation, and angiogenesis in 12Z cells. (A) Western blot results confirmed successful construction of the CEBPD overexpression vector ($p < 0.001$; values are presented as the mean ± SD from a Student's *t*-test; n = 3). (B,C) CEBPD overexpression in 12Z cells to assess changes in MDA and SOD levels (values are shown as the mean ± SD following Student's *t*-test; n = 3). (D) The oxidative stress model was established using hydrogen peroxide (H_2O_2), and the impact of CEPBD overexpression on reactive oxygen species (ROS) levels in 12Z cells was assessed by flow cytometry. (E) The proliferative capacity of 12Z cells was assessed by CCK-8 assay, with the results presented as a line chart ($p < 0.001$; values are presented as the mean ± SD after Student's *t*-test; n = 3). (F) The proliferative capacity was assessed using the clone formation assay, with the bar graphs showing the number of colonies ($p < 0.001$; values are the mean ± SD from a Student's *t*-test; n = 3). Scale bar = 5 mm. (G) The effects of CEBPD overexpression on angiogenesis were analyzed using the chick embryo chorioallantoic membrane (CAM) assay. Red arrows indicate newly formed blood vessels ($p = 0.034$; values represent the mean ± SD from a Student's *t*-test; n = 3). Scale bar = 2 mm. ***$p < 0.001$; *$p < 0.05$.

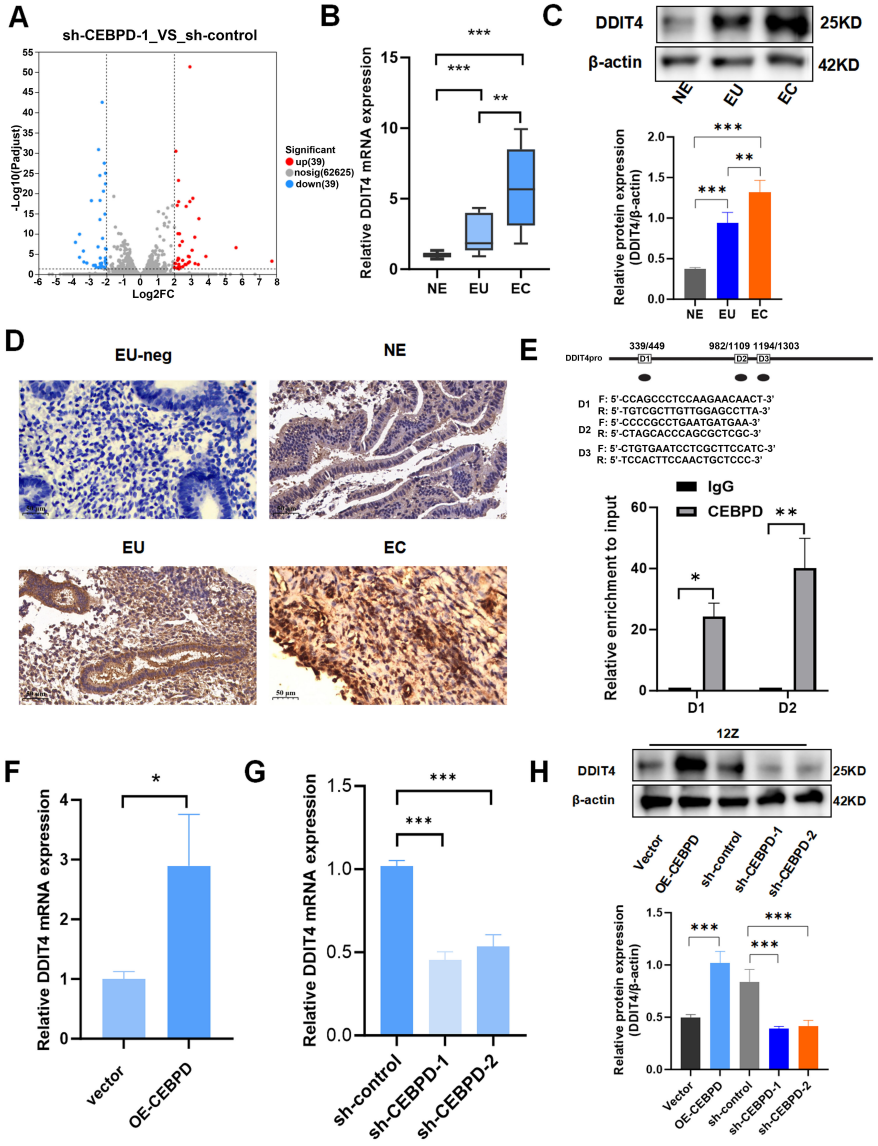

Fig. 4. CEBPD promotes DDIT4 expression in 12Z cells. (A) Differential expression volcano map. Blue dots indicate significantly downregulated genes following shRNA-mediated CEBPD knockdown, whereas red dots represent significantly upregulated genes. X-axis: log2-fold change of gene expression; Y-axis: statistical significance of the differential expression in log10. (B) RT-qPCR analysis was performed to validate *DDIT4* mRNA expression in NE, EU, and EC (NE vs. EC, $p < 0.001$; NE vs. EU, $p < 0.001$; EU vs. EC, $p = 0.02$; Values for *DDIT4* are shown as (M (P25, P75)) following the Kruskal-Wallis test; n = 30). (C) Western blot analysis of DDIT4 expression in EU and EC tissues, and paired NE tissue (NE vs. EC, $p < 0.001$; NE vs. EU, $p = 0.001$; EU vs. EC, $p = 0.007$). Values are presented as the mean ± SD from a one-way ANOVA test; n = 3. (D) Immunohistochemistry showed that DDIT4 was upregulated in EU and EC tissues compared to NE. DDIT4 is detected in both epithelial cells and stromal cells. Scale bar = 50 μm. (E) ChIP-qPCR assay in 12Z cells confirmed that CEBPD was directly correlated with DDIT4 promoters within D1, D2 (D1 $p = 0.011$; D2 $p = 0.002$; values are presented as the mean ± SD from a Student's *t*-test; n = 3). (F) *CEBPD* was first overexpressed in 12Z cells, and then the impact on *DDIT4* mRNA expression was assessed ($p = 0.020$; values are presented as the mean ± SD from a Student's *t*-test; n = 3). (G) Following CEBPD knockdown in 12Z cells, the relative expression of *DDIT4* mRNA was quantified by RT-qPCR (sh-control group vs. sh-CEBPD-1 group, $p < 0.001$; sh-control group vs. sh-CEBPD-2 group, $p < 0.001$; values are presented as the mean ± SD from a one-way ANOVA test; n = 3). (H) CEBPD was overexpressed or knocked down in 12Z cells, and the impact on DDIT4 protein levels was assessed (vector vs. OE-CEBPD, $p < 0.001$; values are presented as the mean ± SD from a Student's *t*-test. sh-control group vs. sh-CEBPD-1 group, $p < 0.001$; sh-control group vs. sh-CEBPD-2 group, $p < 0.001$; values are presented as the mean ± SD from a one-way ANOVA test; n = 3). DDIT4, DNA damage-inducible transcript 4; DEGs, differentially expressed genes; FC, fold change. *$p < 0.05$, **$p < 0.01$, and ***$p < 0.001$.

3.6 CEBPD Promotes Oxidative Stress and Proliferation in EM Through DDIT4 Activation

To further confirm the relationship between CEBPD and DDIT4 in EM, related vectors were constructed as shown in Fig. 5A. Inhibition of CEBPD expression was found to reduce the levels of ROS and MDA significantly, increase SOD activity (Fig. 5B–D), and decrease the proliferation of 12Z cells (Fig. 5E–G). These effects were reversed by DDIT4 supplementation, indicating that CEBPD promotes ectopic endometrial cell oxidative stress and proliferation in EM by activating DDIT4.

3.7 CEBPD Activates the ERK Pathway in Endometriotic Cells via DDIT4

In patients with non-alcoholic steatohepatitis (NASH), DDIT4 may facilitate the assembly of the p38-mitogen-activated protein kinase (MAPK) signaling complex in a S-nitrosylation-dependent manner, thereby enhancing ROS production [17]. We further explored the mechanism that underlies the promoting effect of CEBPD on ectopic endometrial cell proliferation and oxidative stress in EM. *CEBPD* was knocked down in 12Z cells using lentivirus shRNA, producing cell lines in which CEBPD and DDIT4 were significantly downregulated (Fig. 6A,B). Furthermore, the Western blot results indicated that the phospho-ERK (p-ERK) inhibition caused by sh-CEBPD was partially alleviated in the presence of DDIT4 overexpression (Fig. 6C). These results suggest that CEBPD may promote ectopic endometrial cell proliferation and oxidative stress by activating p-ERK activity through DDIT4.

4. Discussion

This study aimed to investigate potential signaling pathways that regulate EM, focusing on oxidative stress pathways. RNA-seq technology was used to analyze normal endometrium from the NE group and eutopic endometrium and ectopic endometrium tissues from patients with EM. This analysis revealed that DEGs were primarily associated with oxidative stress. In combination with an analysis of an online database, CEPBD was found to be highly expressed in eutopic and ectopic tissues, and to promote the generation of ROS in ectopic endometrial cells (12Z cells). The study has reported that the occurrence and progression of EM are closely associated with oxidative stress [18]. Patients suffering severe EM exhibited significantly decreased SOD and glutathione peroxidase activities in both the blood and peritoneal fluid, with the lowest levels found in the peritoneal fluid. Moreover, the MDA level was highest in patients with severe EM [19]. In the present study, CEBPD overexpression in 12Z cells was found to increase the MDA and ROS levels significantly, and to reduce the activity of SOD. Comparatively, knockdown of CEBPD expression had the opposite effect. We searched for evidence that CEBPD was involved in regulating oxidative stress and explored the pathophysiological mechanisms of CEBPD in the development of EM. Our findings indicate that CEBPD promotes the progression of EM by regulating oxidative stress. Few studies have examined the regulation of oxidative stress by CEBPD in endometriosis. In a previous study of EM associated with hypoxia [20], the authors reported increased CEBPD expression in EM tissues compared to normal endometrium, which aligns with the results of the current study. Earlier research found that CEBPD was expressed at high levels in astrocytes, interacts directly with the promoters of NADPH oxidase subunits $p47^{phox}$ and $p67^{phox}$, controls the transcriptional activity of NADPH oxidase, and enhances ROS production [21]. These result in a high level of oxidative stress within the cells, which is believed to be linked to the progression of Alzheimer's disease.

Oxidative stress can lead to pathological changes such as inflammation, angiogenesis, invasive adhesion, cell proliferation, and injury [22]. The present study found that CEBPD overexpression promoted 12Z cell proliferation, alongside oxidative stress and angiogenesis. Furthermore, the loss of CEBPD expression suppressed these observed effects. CEBPD expression is typically reduced in adult tissues, and its abnormal expression has been linked to various cancer types [23]. Initially, CEBPD was observed to inhibit the proliferation of tumor cells, thereby suggesting a role in tumor suppression [24]. However, CEBPD has also been found to mediate cell proliferation in clinical models and cancer patients, and to play a role in tumorigenesis [25]. Thus, it is generally acknowledged that CEBPD fosters an inflammatory environment that encourages tumor development and the recruitment of blood vessels [26]. However, the relationship between CEBPD and EM remains unclear.

RNA-seq analysis revealed that CEBPD might promote endometriotic cell proliferation and oxidative stress by targeting DDIT4. Moreover, ChIP assay results confirmed that CEBPD combined with the *DDIT4* promoter regulates *DDIT4* expression. Thus, *DDIT4* was predicted to be a target for CEBPD. Notably, DDIT4 overexpression significantly rescued the impact of sh-CEBPD on oxidative stress, proliferation, and angiogenesis in endometrial cells. Additionally, Western blot analysis indicated that DDIT4 may promote oxidative stress, proliferation, and angiogenesis of endometrial cells via MAPK signaling. A previous study noted that DDIT4 is a DNA repair factor that supports the rapid proliferation of cells by restoring their ability to repair DNA damage [27]. However, to our knowledge, no relevant studies have yet been conducted on DDIT4 in EM. Most studies on DDIT4 have been conducted in oncology, and numerous authors have shown that DDIT4 may predict disease development and prognosis in various tumor types [28–30]. Moreover, CEBPD has been shown to mediate the development of oxidative stress and inflammation in hypertension [31]. DDIT4 is expressed under stress conditions and regulates cancer cell

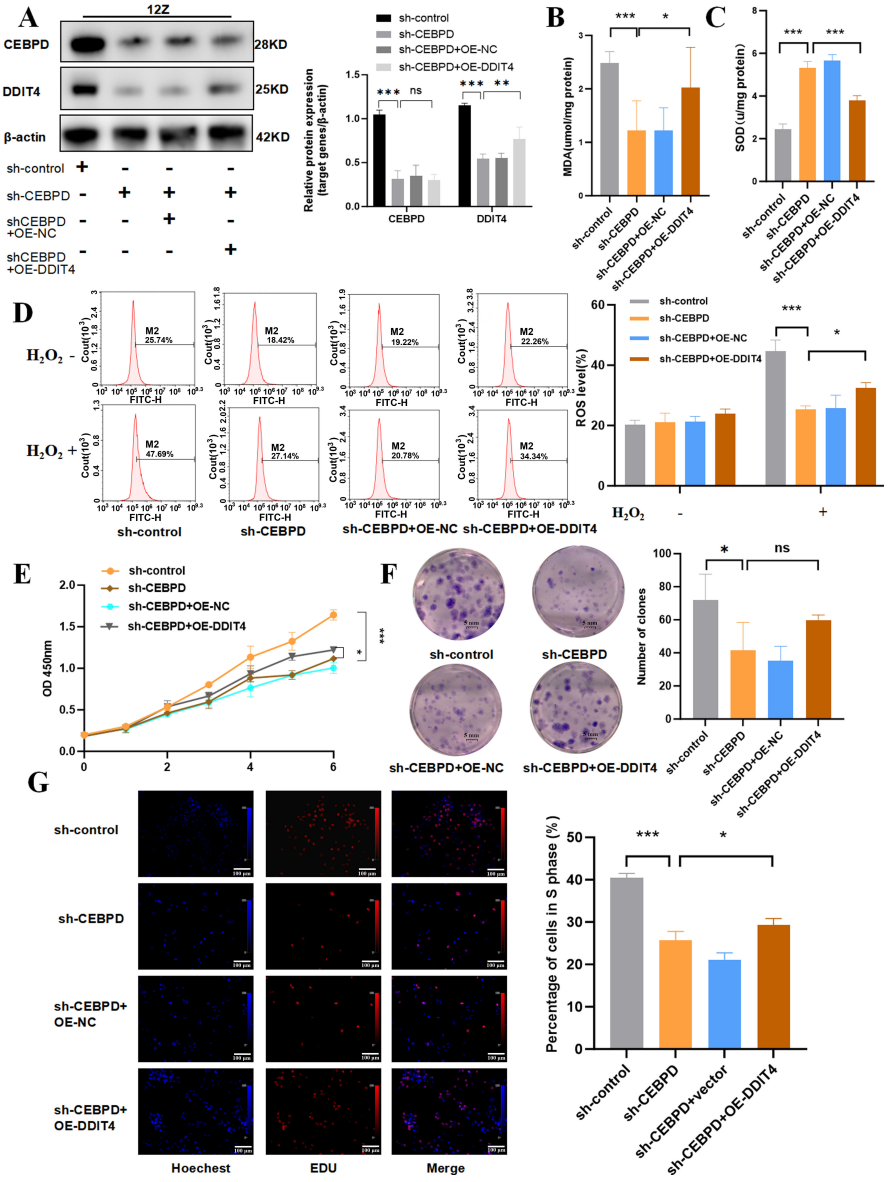

Fig. 5. CEBPD promotes oxidative stress and proliferation by targeting DDIT4 in 12Z cells. (A) The expression levels of CEBPD and DDIT4 in different groups were analyzed by Western blot (the *p*-values for CEBPD and DDIT4 in other groups: sh-control group vs. sh-CEBPD group, $p < 0.001$ and $p < 0.001$; sh-CEBPD group vs. sh-CEBPD + OE-DDIT4 group, $p = 0.825$ and $p = 0.002$; values represent the mean ± SD following one-way ANOVA; n = 3). (B) In the rescue experiment, the level of MDA was assessed in 12Z cells (sh-control group vs. sh-CEBPD group, $p < 0.001$; sh-CEBPD group vs. sh-CEBPD + OE-DDIT4 group, $p = 0.016$; values represent the mean ± SD following one-way ANOVA; n = 6). (C) In the rescue experiment, SOD activity was assessed in 12Z cells (sh-control group vs. sh-CEBPD group, $p < 0.001$; sh-CEBPD group vs. sh-CEBPD + OE-DDIT4 group, $p < 0.001$; values are presented as the mean ± SD following one-way ANOVA; n = 3). (D) The oxidative stress model was constructed in 12Z cells using H_2O_2, and the effect of CEBPD and DDIT4 expression on ROS levels was determined by flow cytometry (sh-control group vs. sh-CEBPD group, $p < 0.001$; sh-CEBPD group vs. sh-CEBPD + OE-DDIT4 group, $p = 0.023$; values represent the mean ± SD after one-way ANOVA; n = 3). (E) The proliferative ability of 12Z cells in different groups was analyzed by CKK-8 (sh-control group vs. sh-CEBPD group, $p < 0.001$; sh-CEBPD group vs. sh-CEBPD + OE-DDIT4 group, $p = 0.030$; values are presented as the mean ± SD from one-way ANOVA; n = 3). (F) The proliferative ability of 12Z cells in different groups was analyzed with the colony formation assay, with bar charts showing the colony numbers (sh-control group vs. sh-CEBPD group, $p = 0.017$; sh-CEBPD group vs. sh-CEBPD + OE-DDIT4 group, $p = 0.109$; values represent the mean ± SD from one-way ANOVA; n = 3). Scale bars = 5 mm. (G) The proliferative ability of 12Z cells in different groups was analyzed using the EdU assay (sh-control group vs. sh-CEBPD group, $p < 0.001$; sh-CEBPD group vs. sh-CEBPD + OE-DDIT4 group, $p = 0.029$; values represent the mean ± SD from one-way ANOVA; n = 3). Scale bars = 100 μm. EdU, 5-Ethynyl-2′-deoxyuridine. *$p < 0.05$, **$p < 0.01$, and ***$p < 0.001$; ns, not significant.

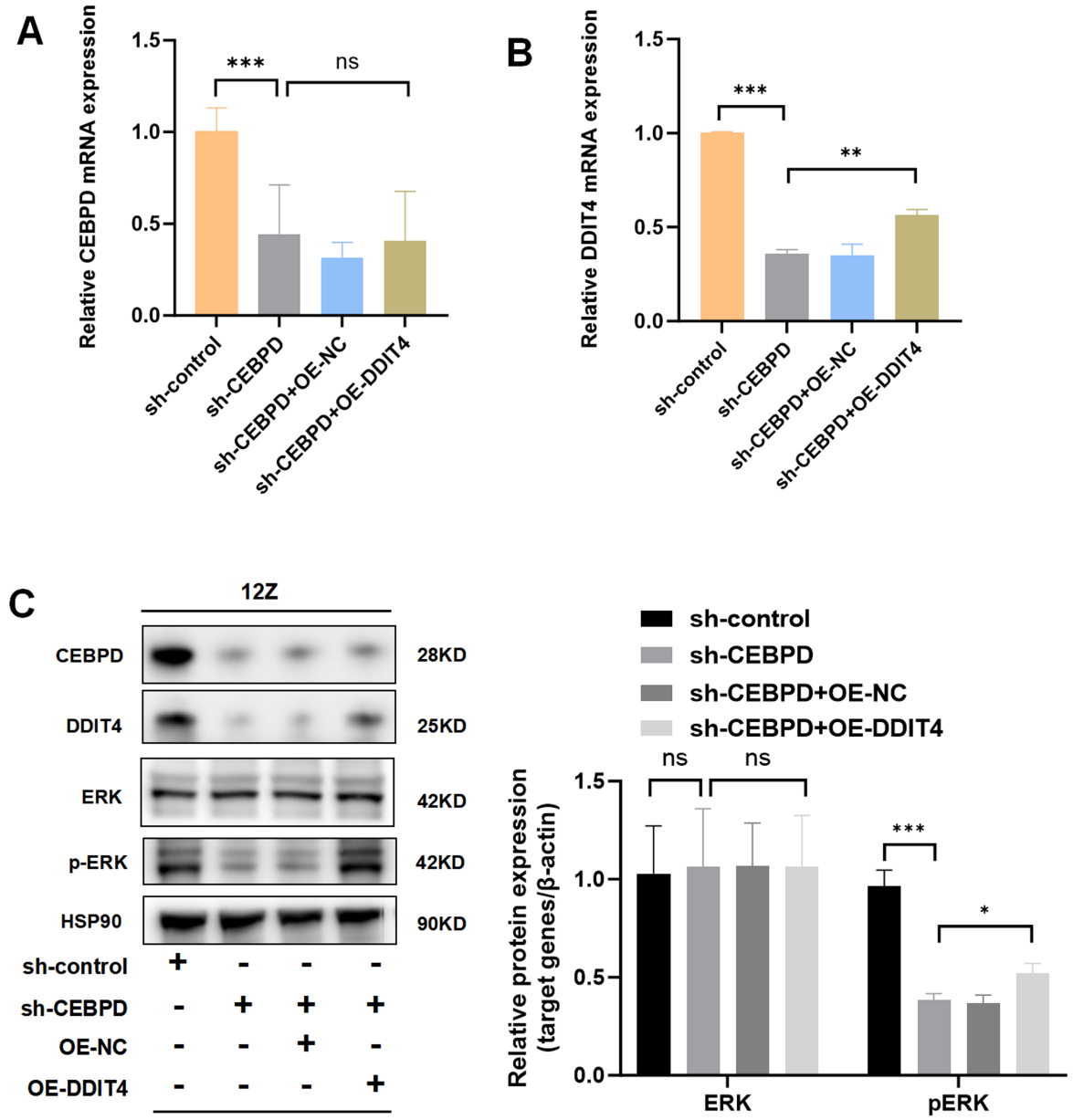

Fig. 6. CEBPD activates the ERK pathway in 12Z cells through DDIT4. (A) The expression of *CEBPD* in different groups was analyzed by RT-qPCR (sh-control group vs. sh-CEBPD group, $p < 0.001$; sh-CEBPD group vs. sh-CEBPD + OE-DDIT4 group, $p = 0.742$; values shown are the mean ± SD following one-way ANOVA; n = 3). (B) The expression of *DDIT4* in different groups was analyzed by RT-qPCR (sh-control group vs. sh-CEBPD group, $p < 0.001$; sh-CEBPD group vs. sh-CEBPD + OE-DDIT4 group, $p = 0.005$; values shown are the mean ± SD after one-way ANOVA; n = 3). (C) The expression of CEBPD, DDIT4, ERK1/2, and p-ERK in different groups was determined by Western blot analysis (the *p*-values for ERK and p-ERK in other groups, sh-control group vs. sh-CEBPD group, $p = 0.874$ and $p < 0.001$; sh-CEBPD group vs. sh-CEBPD + OE-DDIT4 group, $p = 0.993$ and $p = 0.016$; values represent the mean ± SD following one-way ANOVA; n = 3). ERK, extracellular signal-regulated kinase; p-ERK, phospho-ERK. ***$p < 0.001$; **$p < 0.01$; *$p < 0.05$; ns, not significant.

growth by inhibiting mTORC1, an essential protein complex activated by nutrients and hormones [32]. Accordingly, DDIT4 regulates metabolism, oxidative stress, hypoxic survival, and apoptosis [33]. Another recent study found that DDIT4 activated the ROS–TXNIP–NLRP3 axis during oxidative stress-induced pyroptosis in rat nucleus pulposus *in vitro* [34]. Mitochondria are damaged during oxidative stress, and DDIT4 contributes to mitochondrial damage and ROS production. Meanwhile, TXNIP, a well-established key regulator in the cellular stress response [35], has been demonstrated to interact with DDIT4 in modulating oxidative stress pathways. This regulatory mechanism may contribute to the pathogenesis of oxidative stress in EM. However, no direct experimental evidence or clinical

studies have been reported to substantiate this hypothesis in the context of EM.

Although this study provides novel insights into the potential mechanism for oxidative stress-induced EM, several limitations should be acknowledged. First, this *in vitro* study cannot fully simulate the *in vivo* biological complexity of EM; hence, studies using animal models may be more representative. In addition, the existing commercial endometriosis cell line, 12Z cells, may not fully represent EM tissues.

5. Conclusions

The results of this study suggest that CEBPD promotes oxidative stress, cell proliferation, and angiogenesis of endometriotic cells by activating the MAPK signaling pathway.

Availability of Data and Materials

The datasets generated and/or analyzed during the current study are available from the corresponding author upon reasonable request.

Author Contributions

JS: Writing-original draft, Methodology, Formal analysis, Data curation. PT: Validation, Software, Formal analysis, Data curation. JZ: Validation, Software, Methodology. RZ: Formal analysis, Data curation. HX: Supervision, Investigation, Conceptualization. HZ: Research design, Methodology, Data analysis, Manuscript revision. All authors contributed to manuscript writing, critical revision, and approved the final version. All authors have participated sufficiently in the work and agreed to be accountable for all aspects of the work.

Ethics Approval and Consent to Participate

This study was approved by the Ethics Committee of the Huai'an Maternity and Child Health Care Hospital Affiliated to Yangzhou University (License Number: YXYLL-2023-021). The study was conducted in accordance with the Declaration of Helsinki, and all patients or their families/legal guardians were informed of the study and signed an informed consent form. According to the relevant regulations of the "Regulations on the Administration of Laboratory Animals" (revised in 2017) and the "Guidelines for Ethical Review of Animal Welfare" (GB/T 35892-2018) of China, the Chick Embryo Chorioallantoic Membrane Test does not require ethics review and approval.

Acknowledgment

We would like to express our sincere gratitude to all those who provided assistance during the research and writing of this manuscript. Special thanks go to the laboratory staff for their technical support and all the participants in our study. We are also grateful to all the peer reviewers for their valuable opinions and suggestions, which have significantly improved the quality of this manuscript.

Funding

This study was supported by Huai'an City Key Laboratory of Female Fertility Preservation (grant number: HAP202305) and Huai'an Natural Science Foundation (grant number: HAB2024041).

Conflict of Interest

The authors declare no conflict of interest.

Supplementary Material

Supplementary material associated with this article can be found, in the online version, at https://doi.org/10.31083/FBL33488.

References

[1] Salinas-Asensio MDM, Ocón-Hernández O, Mundo-López A, Fernández-Lao C, Peinado FM, Padilla-Vinuesa C, *et al*. 'Physio-EndEA' Study: A Randomized, Parallel-Group Controlled Trial to Evaluate the Effect of a Supervised and Adapted Therapeutic Exercise Program to Improve Quality of Life in Symptomatic Women Diagnosed with Endometriosis. International Journal of Environmental Research and Public Health. 2022; 19: 1738. https://doi.org/10.3390/ijerph19031738.

[2] Sarría-Santamera A, Khamitova Z, Gusmanov A, Terzic M, Polo-Santos M, Ortega MA, *et al*. History of Endometriosis Is Independently Associated with an Increased Risk of Ovarian Cancer. Journal of Personalized Medicine. 2022; 12: 1337. https://doi.org/10.3390/jpm12081337.

[3] Lin SC, Lee HC, Hsu CT, Huang YH, Li WN, Hsu PL, *et al*. Targeting Anthrax Toxin Receptor 2 Ameliorates Endometriosis Progression. Theranostics. 2019; 9: 620–632. https://doi.org/10.7150/thno.30655.

[4] Kapoor R, Stratopoulou CA, Dolmans MM. Pathogenesis of Endometriosis: New Insights into Prospective Therapies. International Journal of Molecular Sciences. 2021; 22: 11700. https://doi.org/10.3390/ijms222111700.

[5] Yoshikawa T, You F. Oxidative Stress and Bio-Regulation. International Journal of Molecular Sciences. 2024; 25: 3360. https://doi.org/10.3390/ijms25063360.

[6] Samimi M, Pourhanifeh MH, Mehdizadehkashi A, Eftekhar T, Asemi Z. The role of inflammation, oxidative stress, angiogenesis, and apoptosis in the pathophysiology of endometriosis: Basic science and new insights based on gene expression. Journal of Cellular Physiology. 2019; 234: 19384–19392. https://doi.org/10.1002/jcp.28666.

[7] Huang YJ, Nan GX. Oxidative stress-induced angiogenesis. Journal of Clinical Neuroscience: Official Journal of the Neurosurgical Society of Australasia. 2019; 63: 13–16. https://doi.org/10.1016/j.jocn.2019.02.019.

[8] Zhu S, Wang A, Xu W, Hu L, Sun J, Wang X. The heterogeneity of fibrosis and angiogenesis in endometriosis revealed by single-cell RNA-sequencing. Biochimica et Biophysica Acta. Molecular Basis of Disease. 2023; 1869: 166602. https://doi.org/10.1016/j.bbadis.2022.166602.

[9] Yin M, Zhai L, Wang J, Yu Q, Li T, Xu X, *et al*. Comprehensive Analysis of RNA-Seq in Endometriosis Reveals Competing Endogenous RNA Network Composed of circRNA, lncRNA

and mRNA. Frontiers in Genetics. 2022; 13: 828238. https://doi.org/10.3389/fgene.2022.828238.

[10] Bi J, Wang D, Cui L, Yang Q. RNA sequencing-based long non-coding RNA analysis and immunoassay in ovarian endometriosis. American Journal of Reproductive Immunology (New York, N.Y.: 1989). 2021; 85: e13359. https://doi.org/10.1111/aji.13359.

[11] Wang D, Ruan X, Liu X, Xue Y, Shao L, Yang C, *et al*. SUMOylation of PUM2 promotes the vasculogenic mimicry of glioma cells via regulating CEBPD. Clinical and Translational Medicine. 2020; 10: e168. https://doi.org/10.1002/ctm2.168.

[12] Liu D, Zhang XX, Li MC, Cao CH, Wan DY, Xi BX, *et al*. C/EBPβ enhances platinum resistance of ovarian cancer cells by reprogramming H3K79 methylation. Nature Communications. 2018; 9: 1739. https://doi.org/10.1038/s41467-018-03590-5.

[13] Wang YH, Wu WJ, Wang WJ, Huang HY, Li WM, Yeh BW, *et al*. CEBPD amplification and overexpression in urothelial carcinoma: a driver of tumor metastasis indicating adverse prognosis. Oncotarget. 2015; 6: 31069–31084. https://doi.org/10.18632/oncotarget.5209.

[14] Gardiner JD, Abegglen LM, Huang X, Carter BE, Schackmann EA, Stucki M, *et al*. C/EBPβ-1 promotes transformation and chemoresistance in Ewing sarcoma cells. Oncotarget. 2017; 8: 26013–26026. https://doi.org/10.18632/oncotarget.14847.

[15] Sowamber R, Chehade R, Bitar M, Dodds LV, Milea A, Slomovitz B, *et al*. CCAAT/enhancer binding protein delta (C/EBPδ) demonstrates a dichotomous role in tumour initiation and promotion of epithelial carcinoma. EBioMedicine. 2019; 44: 261–274. https://doi.org/10.1016/j.ebiom.2019.05.002.

[16] Livak KJ, Schmittgen TD. Analysis of relative gene expression data using real-time quantitative PCR and the 2(-Delta Delta C(T)) Method. Methods. 2001; 25: 402–408. https://doi.org/10.1006/meth.2001.1262.

[17] Li Z, Zhao Q, Lu Y, Zhang Y, Li L, Li M, *et al*. DDIT4 S-nitrosylation aids p38-MAPK signaling complex assembly to promote hepatic reactive oxygen species production. Advanced Science [published correction in Advanced Science. 2022; 9: 2201652. https://doi.org/10.1002/advs.202201652]. 2021; 8: e2101957. https://doi.org/10.1002/advs.202101957.

[18] Ding J, Mei S, Wang K, Cheng W, Sun S, Ni Z, *et al*. Curcumin modulates oxidative stress to inhibit pyroptosis and improve the inflammatory microenvironment to treat endometriosis. Genes & Diseases. 2023; 11: 101053. https://doi.org/10.1016/j.gendis.2023.06.022.

[19] Amreen S, Kumar P, Gupta P, Rao P. Evaluation of Oxidative Stress and Severity of Endometriosis. Journal of Human Reproductive Sciences. 2019; 12: 40–46. https://doi.org/10.4103/jhrs.JHRS_27_17.

[20] Rytkönen KT, Heinosalo T, Mahmoudian M, Ma X, Perheentupa A, Elo LL, *et al*. Transcriptomic responses to hypoxia in endometrial and decidual stromal cells. Reproduction (Cambridge, England). 2020; 160: 39–51. https://doi.org/10.1530/REP-19-0615.

[21] Wang SM, Lim SW, Wang YH, Lin HY, Lai MD, Ko CY, *et al*. Astrocytic CCAAT/Enhancer-binding protein delta contributes to reactive oxygen species formation in neuroinflammation. Redox Biology. 2018; 16: 104–112. https://doi.org/10.1016/j.redox.2018.02.011.

[22] Vallée A, Lecarpentier Y. Curcumin and Endometriosis. International Journal of Molecular Sciences. 2020; 21: 2440. https://doi.org/10.3390/ijms21072440.

[23] Chan TC, Shiue YL, Li CF. The biological impacts of CEBPD on urothelial carcinoma development and progression. Frontiers in Oncology. 2023; 13: 1123776. https://doi.org/10.3389/fonc.2023.1123776.

[24] Hartl L, Duitman J, Aberson HL, Chen K, Dijk F, Roelofs JJTH, *et al*. CCAAT/Enhancer-Binding Protein Delta (C/EBPδ): A Previously Unrecognized Tumor Suppressor that Limits the Oncogenic Potential of Pancreatic Ductal Adenocarcinoma Cells. Cancers. 2020; 12: 2546. https://doi.org/10.3390/cancers12092546.

[25] Mao XG, Xue XY, Lv R, Ji A, Shi TY, Chen XY, *et al*. CEBPD is a master transcriptional factor for hypoxia regulated proteins in glioblastoma and augments hypoxia induced invasion through extracellular matrix-integrin mediated EGFR/PI3K pathway. Cell Death & Disease. 2023; 14: 269. https://doi.org/10.1038/s41419-023-05788-y.

[26] Spek CA, Aberson HL, Butler JM, de Vos AF, Duitman J. CEBPD Potentiates the Macrophage Inflammatory Response but CEBPD Knock-Out Macrophages Fail to Identify CEBPD-Dependent Pro-Inflammatory Transcriptional Programs. Cells. 2021; 10: 2233. https://doi.org/10.3390/cells10092233.

[27] Foltyn M, Luger AL, Lorenz NI, Sauer B, Mittelbronn M, Harter PN, *et al*. The physiological mTOR complex 1 inhibitor DDIT4 mediates therapy resistance in glioblastoma. British Journal of Cancer. 2019; 120: 481–487. https://doi.org/10.1038/s41416-018-0368-3.

[28] Yoshikawa N, Yoshida K, Liu W, Matsukawa T, Hattori S, Yoshihara M, *et al*. The prognostic significance of DDIT4 in endometrial cancer. Cancer Biomarkers: Section a of Disease Markers. 2023; 37: 217–225. https://doi.org/10.3233/CBM-220368.

[29] Fattahi F, Zanjani LS, Shams ZH, Kiani J, Mehrazma M, Najafi M, *et al*. High Expression of DNA Damage-Inducible Transcript 4 (DDIT4) Is Associated with Advanced Pathological Features in Patients with Colorectal Cancer. Scientific Reports. 2021; 11: 13626. https://doi.org/10.1038/s41598-021-92720-z.

[30] Carew JS, Espitia CM, Sureshkumar S, Espinoza MJC, Gamble ME, Wang W, *et al*. REDD1 is a Determinant of the Sensitivity of Renal Cell Carcinoma Cells to Autophagy Inhibition that can be Therapeutically Exploited by Targeting PIM Activity. Cancer Letters. 2025; 613: 217496. https://doi.org/10.1016/j.canlet.2025.217496.

[31] Zhao J, Hu J, Zhang R, Deng J. CEBPD Regulates Oxidative Stress and Inflammatory Responses in Hypertensive Cardiac Remodeling. Shock (Augusta, Ga.). 2023; 60: 713–723. https://doi.org/10.1097/SHK.0000000000002228.

[32] Tirado-Hurtado I, Fajardo W, Pinto JA. DNA Damage Inducible Transcript 4 Gene: The Switch of the Metabolism as Potential Target in Cancer. Frontiers in Oncology. 2018; 8: 106. https://doi.org/10.3389/fonc.2018.00106.

[33] Naki M, Gourdomichali O, Zonke K, Kattan FG, Makridakis M, Kontostathi G, *et al*. APEX2-Mediated Proximity Labeling Resolves the DDIT4-Interacting Proteome. International Journal of Molecular Sciences. 2022; 23: 5189. https://doi.org/10.3390/ijms23095189.

[34] Ma M, Zhang C, Zhong Z, Wang Y, He X, Zhu D, *et al*. siRNA Incorporated in Slow-Release Injectable Hydrogel Continuously Silences DDIT4 and Regulates Nucleus Pulposus Cell Pyroptosis Through the ROS/TXNIP/NLRP3 Axis to Alleviate Intervertebral Disc Degeneration. Bone Joint Research. 2024; 13: 247–260. https://doi.org/10.1302/2046-3758.135.BJR-2023-0320.R1.

[35] Choi EH, Park SJ. TXNIP: A key protein in the cellular stress response pathway and a potential therapeutic target. Experimental & Molecular Medicine. 2023; 55: 1348–1356. https://doi.org/10.1038/s12276-023-01019-8.